Imaging Lymphoid Cell Death In Vivo During Polymicrobial Sepsis*

Lin Zou, MD[1], **Howard H. Chen, PhD**[2], **Dan Li, MD**[1], **Ganqiong Xu, MD**[1], **Yan Feng, MD, PhD**[1], **Chan Chen, MD, PhD**[1], **Larry Wang, MD**[3], **David E. Sosnovik, MD**[2], **Wei Chao, MD, PhD**[1]

[1]Department of Anesthesia, Critical Care and Pain Medicine, Massachusetts General Hospital, Harvard Medical School, Boston, MA.

[2]Martinos Center for Biomedical Imaging, Department of Radiology, Massachusetts General Hospital, Harvard Medical School, Boston, MA.

[3]Department of Pathology and Laboratory Medicine, Children's Hospital Los Angeles, Los Angeles, CA.

Abstract

Objectives: Cell death in lymphatic organs, such as the spleen, is in part responsible for immunosuppression and contributes to mortality during sepsis. An early and noninvasive detection of lymphoid cell death could thus have significant clinical implications. Here, we tested in vivo imaging of lymphoid cell death using a near-infrared annexin V (AV-750).

Design: Animal study.

Setting: Laboratory investigation.

Subjects: C57BL/6J wild-type and toll-like receptor 3 knockout mice.

Interventions: Mild and severe polymicrobial sepsis was induced with cecum ligation and puncture. Serum cytokines and acute kidney injury markers were tested by immunoassay and quantitative reverse transcription-polymerase chain reaction, respectively. Sepsis-induced lymphoid cell death was detected by fluorescent AV-750 accumulation in the thorax and abdomen (in vivo), in isolated organs (ex vivo), and in isolated cells (flow cytometry). Caspase-3 cleavage/ activity and terminal deoxynucleotidyl transferase dUTP nick-end labeling staining were tested for apoptosis.

Measurements and Main Results: Severe sepsis induced marked apoptosis in the thymus, spleen, and liver as demonstrated by cleaved caspase-3 and an increase in caspase-3 activity and

terminal deoxynucleotidyl transferase dUTP nick-end labeling–positive cells. A significant increase in fluorescent AV-750 signal was seen in the thoracic and upper abdominal fields and associated with the severity of sepsis. The in vivo thoracic and abdominal AV-750 fluorescent signal was attributed to the thymus, liver, and spleen as determined by ex vivo imaging and highly correlated with the levels of cell death in thymocytes and splenocytes, respectively, as measured by flow cytometry. Compared with wild-type septic mice, toll-like receptor 3 septic mice had attenuated abdominal AV-750 fluorescent signal, reduced ex vivo fluorescence in the spleen, and decreased splenocyte cell death.

Conclusions: In vivo AV-750 fluorescent imaging provides spatially resolved and organ-specific detection of lymphoid cell death during polymicrobial sepsis. The AV-750 fluorescent intensity in the thoracic and abdominal fields is associated with sepsis severity and well correlated with sepsis-induced cell death in the thymus and spleen, respectively. *(Crit Care Med* 2015; 43:2303–2312)

Keywords

apoptosis; imaging; immunosuppression; lymphocyte cell death; necrosis; sepsis

Sepsis is the 10th leading cause of death (1). In the United States, sepsis develops in 750,000 people annually, and more than 210,000 of these patients do not survive (2). Unfortunately, specific and effective strategies for sepsis management are currently unavailable, and the mortality from sepsis thus remains unacceptably high. Initial sepsis therapy aims to attenuate hyperinflammation in the early stage with poor outcomes (3–5). Recent studies have implicated the pivotal role of immune cell death in the immunosuppression and pathogenesis of sepsis (6, 7). Therefore, developing a diagnostic tool to detect and quantify cell death early in vivo during sepsis has a potential clinical implication.

Hotchkiss et al (8) have documented a marked decrease in the levels of B cells, CD4 T cells, and follicular dendritic cells in patients with severe sepsis. Autopsy studies in patients who had died of sepsis disclosed a severe loss of cells of the adaptive immune system. Lymphocyte apoptosis most often occurs in lymphoid tissues, such as the spleen and thymus (9). In a prospective study (7), investigators found that more than 50% of septic patients had a significant number of apoptotic lymphocytes in the spleens and more than 10–20% splenic cells were apoptotic, whereas there was minimal splenic cell death in patients who died of nonseptic critical illness. In a bowel perforation model of sepsis, a significant number of apoptotic cells were seen in the liver and spleen (10, 11). Thus, blocking lymphocyte cell death, improving immunological competence, and strengthening the immune function of septic patients may represent an attractive strategy for the management of a subset of septic patients (12, 13).

Among different types of cell death, apoptosis and necrosis are the most commonly described. The central component of apoptosis is a proteolytic system involving a family of proteases called "caspases." The significance of cellular apoptosis in the pathogenesis of sepsis is demonstrated by the fact that caspase inhibition markedly improves survival of septic animals (14, 15). One of the early events of apoptosis includes translocation of membrane phosphatidylserine from the inner side of the plasma membrane to the cell surface (16–18). Phosphatidylserine translocation precedes the loss of membrane integrity,

which accompanies the later stages of cell death resulting in either apoptotic or necrotic processes. Annexin V, a Ca^{2+}-dependent phospholipid-binding protein, has a high affinity for phosphatidylserine (19) and retains its high affinity for phosphatidylserine when conjugated with fluorochromes (18, 19). Importantly, annexin V appears to detect apoptosis-associated membrane changes on live cells before the nuclear condensation events that occur during this process (18). Under necrotic conditions, however, annexin V penetrates through the damaged plasma membrane and binds to the inner leaflet phosphatidylserine. Therefore, annexin V can serve as a sensitive probe to detect cell death.

This study was designed to test the utility of detecting lymphoid cell death in vivo noninvasively using fluorescence-labeled annexin V (AV-750) in a mouse model of polymicrobial sepsis. Specifically, we tested the ability of AV-750 to assess the severity of sepsis and the sepsis-induced lymphoid cell death in the thymus and spleen. We further investigated the ability of annexin V in vivo imaging to determine the protective effect of toll-like receptor 3 (TLR3) deficiency against sepsis-induced lymphoid cell death.

METHODS

Animals

Eight- to 12-week-old gender- and age-matched mice were used for the studies. C57BL/6J wild-type (WT) and TLR3$^{-/-}$ mice were purchased from the Jackson Laboratories and housed in a Massachusetts General Hospital (MGH) animal facility for at least 1 week before experiments. All animals were housed in pathogen-free, temperature-controlled, and air-conditioned facilities with light/dark cycles (12 hr/12 hr) and fed with the same bacteria-free diet. All animal care and procedures were performed according to the protocols approved by the Subcommittee on Research Animal Care of MGH and are in compliance with the "Guide for the Care and Use of Laboratory Animals" published by the National Institutes of Health.

Mouse Model of Polymicrobial Sepsis

A clinically relevant rodent model of sepsis was created by cecum ligation and puncture (CLP) as has been described previously (20–22). In brief, mice were anesthetized with ketamine (100 mg/kg) and xylazine (4 mg/kg). The abdominal cavity was opened in layers. The cecum was ligated 1.0 cm from the tip and punctured through to through with a 27- or 18-gauge needle to generate a mild or severe model of polymicrobial sepsis. A small amount of fecal materials was squeezed out gently before the ligated cecum was returned to the abdominal cavity. The sham-operated mice underwent laparotomy but without CLP. After surgery, prewarmed normal saline (0.05 mL/g body weight) was administered subcutaneously. Postoperative pain control was managed with subcutaneous injection of bupivacaine (3 mg/kg) and buprenorphine (0.1 mg/kg).

Mortality

WT mice subjected to sham or CLP procedures were observed every 6 hours during the first 2 days and every 12 hours thereafter for up to 168 hours.

Cell Death Imaging With Annexin V

Image Acquisition.—Fluorescence reflectance imaging (FRI) of apoptosis was performed using a commercially available near-infrared (NIR) fluorescent annexin V (Annexin-Vivo 750 = AV-750, Perkin Elmer, Waltham, MA), suitable for in vivo imaging. The light at the wavelength needed to excite and visualize the signal can penetrate 4–5 cm into tissue, and thus, it is able to image cell death in vivo in the mouse model. Mice were injected via the tail vein with 100 μL of AV-750 as per manufacturer's instruction 20 hours after surgery. Four hours later, mice were anesthetized with ketamine (100 mg/kg, IP) and had hair removed from the chest and abdomen. For AV-750 imaging, anesthetized mice were placed in a supine position on a heated stage in the IVIS Spectrum imager (Perkin Elmer). FRI images for AV-750 were acquired with 745-nm excitation and 800-nm emission filter settings on an IVIS Spectrum system (Perkin Elmer). After imaging, mice were euthanized and the thymus, spleen, liver, blood, and heart were harvested and immediately imaged ex vivo with the same filter settings.

Image Analysis.—AV-750 signal was quantified by measuring the signal intensity within a defined region of interest (ROI) described below. For in vivo imaging, three ROIs were applied to each mouse: 1) an ROI of at least 54.4 mm^2 was placed over the thorax, 2) an ROI greater than 475.5 mm^2 was placed over the abdomen, and 3) an ROI was placed over the bladder. For ex vivo imaging, an ROI was defined by manually tracing the edges of the tissue. Mean fluorescence intensity was tabulated for each ROI and normalized to the sham-operated animal to determine fold change. Image analysis was performed in Image J (National Institutes of Health, Bethesda, MD).

Flow Cytometry

After ex vivo imaging, the thymus and spleen were gently ground, and thymocytes and splenocytes filtered through a 70-μm cell strainer with phosphate-buffered saline (PBS). Residual RBCs in the suspension were lysed by RBC lysis buffer containing ammonium chloride (eBioscience, San Diego, CA) followed by washing in PBS. Cells (5×10^5) were suspended in annexin V–binding buffer (BD Biosciences, San Jose, CA) and labeled with fluorescein-labeled annexin V (BD Biosciences) and propidium iodide (PI) (Roche Diagnostics, Indianapolis, IN). Identification of apoptotic or necrotic cells was performed with flow cytometry.

Caspase-3 Activity

Twelve hours after surgery, the thymus, spleen, and liver were harvested and immediately frozen in liquid nitrogen. Tissue powder was suspended in ice-cold lysis buffer provided by a caspase-3 fluorescence assay kit (R&D Systems, Minneapolis, MN). The same amount of protein was assayed for caspase-3 activity as described previously (23).

Terminal Deoxynucleotidyl Transferase dUTP NickEnd Labeling Assay

Twenty-four hours after surgery, the liver, spleen, and thymus were harvested and fixed with 4% formaldehyde overnight and embedded in paraffin. Tissue sections were rehydrated via a graded ethanol series: 95%, 90%, 80%, and 70% ethanol sequentially. Terminal

deoxynucleotidyl transferase dUTP nick-end labeling (TUNEL) staining was performed following the manufacturer's instructions with In Situ Cell Death Detection Kit (Roche Diagnostics).

Western Blot

Animal were euthanized, and organs quickly frozen in liquid nitrogen. Tissue powders were suspended in NP-40 lysis buffer supplemented with complete protease inhibitor cocktails (Roche Diagnostics) and incubated at 4°C for 45 minutes with vortex every 15 minutes. Tissue lysates were then centrifuged, and the supernatants were quantified for protein concentration by Bradford method. Tissue proteins were fractionated by sodium dodecyl sulfate polyacrylamide gel electrophoresis under reducing conditions and blotted with rabbit anti-mouse cleaved cas-pase-3 antibody (Cell Signaling, Danvers, MA). Horseradish peroxidase (HRP)–conjugated anti-rabbit IgG (Cell signaling) was used as the secondary antibody. Glyceraldehyde-3-phosphate dehydrogenase (GAPDH) protein was served as protein loading control. Bands were visualized using Luminata Forte Western HRP substrate (Millipore, Billerica, MA).

Quantitative Reverse Transcription-Polymerase Chain Reaction

RNA was extracted using TRIzol reagent, and complementary DNA was synthesized by reverse-transcriptase reaction. Messenger RNA was quantified using quantitative reverse transcription-polymerase chain reaction (PCR) as described previously (21). The following PCR primers were used: mouse GAPDH: forward 5′-AACTTTGGCATTGTGGAAGG-3′, reverse 5′-GGATGCAGGGATGATGTTCT-3′; mouse neutrophil gelatinase–associated lipocalin (NGAL) (24): forward 5′-CTCAGAACTTGATCCCTGCC-3′, reverse 5′-TCCTTGAG-GCCCAGAGACTT-3′; mouse kidney injury molecule-1 (KIM-1) (24): forward 5′-CATTTAGGCCTCATACTGC-3′, reverse 5′-ACAAGCAGAAGATGGGCATT-3′.

Multiplex Cytokine Immunoassays

Twenty-four hours after surgery, blood was collected through cardiac puncture. Sera were prepared after 1,000g of centrifugation for 10 minutes at 4°C and stored at −80°C. Cytokine concentrations were determined using a fluorescent bead–based multiplex immunoassay (Luminex, Austin, TX) as previously described (20, 25). Briefly, antibody for each cytokine was covalently immobilized to a set of fluorescent microspheres according to manufacturer's instruction (Millipore). After overnight incubation, cytokines bound on the surface of microspheres were detected by a cocktail of biotinylated antibodies. Following binding of streptavidin-phycoerythrin conjugates, the reporter fluorescent signal was measured using a Luminex 200 reader (Luminex). Final cytokine concentrations were calculated based on a standard cytokine curve obtained in each experiment.

Statistical Analysis

Statistical analysis was performed using GraphPad Prism 5 software (GraphPad Software, La Jolla, CA). The distributions of the continuous variables were expressed as mean ± SE. The comparison among sham, mild, and severe sepsis was analyzed by one-way analysis of

variance with Tukey post hoc test. The survival data were analyzed with a log-rank test. Student *t* test was used for statistical analysis between groups of all other data. Of note, these specific comparisons were made based on a priori hypotheses rather than pure statistic considerations. The null hypothesis was rejected for *p* less than 0.05 with the two-tailed test.

RESULTS

Polymicrobial Sepsis Leads to Marked Cellular Apoptosis in the Liver, Spleen, and Thymus

As shown in Figure 1A, CLP was associated with a marked increase in cleaved caspase-3 in the liver, spleen, and thymus of septic mice when compared with that of sham mice. Caspase-3 activity was also increased by 3-, 4.6-, and 8.4-fold in the septic liver, spleen, and thymus compared with those of sham organs (Fig. 1B), indicating significant apoptotic activation in these septic organs at 24 hours after surgery. Consistently, there was a marked increase in the TUNEL-positive cells in the septic liver, spleen, and thymus, further confirming that substantial amounts of apoptosis were produced by sepsis in the mice (Fig. 1C).

Creating Two Mouse Models of Polymicrobial Sepsis

To explore the diagnostic value of annexin V in lymphoid cell death detection during sepsis, we created two CLP models of sepsis at different levels of severity. Circulating cytokines, such as interleukin (IL)-6, are known to contribute to septic mortality (26) and therefore reflect sepsis severity (27). As shown in Figure 2, in mice with mild sepsis, circulating cytokines, including IL-6, keratinocyte chemoattractant, and monocyte chemoattractant protein-1, were modestly but significantly increased when compared with that of the sham mice. In comparison, mice with severe sepsis exhibited significantly higher levels of these cytokines (Fig. 2A). Kidney NGAL and KIM-1, two sensitive markers for acute kidney injury (24, 28–30), were also significantly up-regulated in septic mice. The elevation of these acute kidney injury markers was also associated with the severity level of sepsis with the highest level of the biomarkers in mice with severe sepsis (Fig. 2B), indicating that the degree of acute kidney injury was consistent with the overall severity of sepsis. Finally, the mortality data validated the different levels of severity in the two models of sepsis. While no mice died in the sham group, severe sepsis group had a mortality of 50% at 48 hours and mild sepsis group had a mortality of 20% (Fig. 2C).

Annexin V Imaging of Cell Death During Sepsis

Twenty hours after sham or CLP surgery, AV-750 dye was administered IV, and whole-body fluorescent images were obtained 4 hours later. As shown in Figure 3, A and B, there was significantly higher uptake of AV-750 fluorescence signal in both mild and severe septic mice compared with the sham mice. Normalized AV-750 fluorescence signal in the thorax increased significantly in the mild CLP mice compared with sham (1.20 ± 0.07; $p < 0.05$) and further increased in the severe CLP mice (1.43 ± 0.06; $p < 0.0001$ vs sham). The increased fluorescent signal was attributed to the thymus (Fig. 3C) as the heart and blood produced no signal increase compared with the sham mice (Supplemental Fig. 1 A–C, Supplemental Digital Content 1, http://links.lww.com/CCM/B394), and the lung did not generate any detectable fluorescent signal in the septic mice (Supplemental Fig. 1D,

Supplemental Digital Content 1, http://links.lww.com/CCM/B394). In the upper abdominal field, the increase in AV-750 signal was also observed in the mild (1.16 ± 0.07) and severe sepsis (1.34 ± 0.07; $p < 0.001$) groups (Fig. 3B). Interestingly, bladder signal in the CLP mice decreased in both the mild (0.55 ± 0.12; $p < 0.01$) and the severe sepsis (0.66 ± 0.10; $p < 0.01$) groups.

To determine the organ accumulation of AV-750 in septic mice, we isolated thymus, spleen, and liver for ex vivo fluorescent imaging. As shown in Figure 3C, there was an increase in AV-750 signal in all three organs isolated from the septic mice compared with those of the sham mice. The quantitative data suggest that AV-750 signal was significantly increased in the spleen (mild, 1.56 ± 0.21; severe, 3.35 ± 0.52; $p < 0.001$ vs sham) and liver (mild, 1.07 ± 0.06; severe, 1.73 ± 0.06; $p < 0.0001$ vs sham) of septic mice (Fig. 3D). Of note, in the thymus, both mild and severe sepsis generated significantly higher AV-750 signal independent of severity at 24 hours (Fig. 3, C and D), indicating that thymus was most susceptible to sepsis-induced cell death.

Flow Cytometry Validation of AV-750 Imaging of Sepsis-Induced Apoptosis

To validate and quantify cell death in the septic organs, immediately after ex vivo AV-750 imaging, we isolated thymocytes and splenocytes from sham and CLP mice and tested them for apoptotic and necrotic cell death with fluorescein isothiocyanate–labeled annexin V (AX) and PI by flow cytometry. As illustrated in Figure 4A, three groups of cells were identified by flow cytometry: 1) live cells ($AX^- PI^-$), 2) early apoptotic cells ($AX^+ PI^-$), and 3) late apoptotic and necrotic cells ($AX^+ PI^+$). Sham mice had a basal level (14%) of cell death in thymocytes (Fig. 4, A and B) and 10.5% in splenocytes (including all AX^+ cells = $AX^+ PI^-$ and $AX^+ PI^+$) (Fig. 4, C and D), most likely caused by the cell isolation process. CLP induced a marked increase in AX^+ cell population with approximately 60% in the mild group and 57% in the severe group in thymocytes (mild vs sham: $60\% \pm 4.6\%$ vs $14\% \pm 1.4\%$, $p < 0.001$; severe vs sham: $56.9\% \pm 5.4\%$ vs $14\% \pm 1.4\%$, $p < 0.001$) (Fig. 4, A and B), which was consistent with the ex vivo thymus AV-750 imaging in Figure 3, C and D. In splenocytes (Fig. 4, C and D), the severe sepsis group led to more cell death than the mild sepsis group with AX^+ population around 24% in severe and 18% in mild groups (severe vs sham: $23.9\% \pm 6.8\%$ vs $10.5\% \pm 1.1\%$, $p < 0.05$; mild vs sham: $18.1\% \pm 3.4\%$ vs $10.5\% \pm 1.1\%$) (Fig. 4, C and D). Importantly, these results were consistent with the AV-750 signal in in vivo abdominal area (Fig. 3, A and B) and ex vivo spleen imaging (Fig. 3, C and D). Furthermore, there appeared a significant correlation between the level of cell death as measured by flow cytometry in isolated cells and the in vivo or ex vivo AV-750 imaging (Fig. 4, E and F). Specifically, there was a good correlation between thoracic or thymus AV-750 imaging and AX^+ thymocytes or between abdominal or spleen AV-750 imaging and AX^+ splenocytes (Fig. 4, E and F). These results indicate that AV-750 in vivo imaging accurately detects cell death in these deep parenchymal organs during polymicrobial sepsis. Finally, the peripheral lymphocyte and granulocyte numbers were markedly reduced in both mild and severe septic models (Fig. 4G).

TLR3 Deficiency Leads to Reduction in Cell Death in the Spleen During Polymicrobial Sepsis

We next tested the effect of TLR3 deficiency on lymphoid cell death during sepsis using AV-750 imaging. TLR3 is the sensor for double-stranded RNA and is well known for its role in the host antiviral defense (31, 32). As indicated in Figure 5, A and B, there was a marked increase in thoracic and abdominal AV-750 signals in WT CLP mice compared with WT sham mice. Compared with WT-CLP mice, TLR3$^{-/-}$-CLP mice had a significant reduction in the abdominal fluorescence (TLR3$^{-/-}$-CLP vs WT-CLP; $p < 0.01$), whereas no significant difference was seen in the thoracic region. AV-750 imaging of the isolated thymus and spleen revealed a marked increase in AV-750 signals in CLP animals compared with that of the sham animals (Fig. 5, C and D). When imaged ex vivo, TLR3$^{-/-}$ septic mice had attenuated the AV-750 signal in the spleen but not in the thymus, compared with WT septic mice (Fig. 5, C and D). Of note, both WT and TLR3$^{-/-}$ sham mice had the same basal level of AV-750 signaling in vivo and in vitro (data not shown). Similarly, flow cytometry analysis showed similar results as the ex vivo AV-750 imaging. The basal level of cell death is similar between WT and TLR3$^{-/-}$ sham mice in both thymocytes and splenocytes. Thymocytes from both WT and TLR3$^{-/-}$ septic mice showed a similar level of increase in dead cell population (AX$^+$%) compared with that of the sham (Fig. 5, E and F). Splenocytes from WT septic mice displayed a significant increase in apoptotic (AX$^+$/PI$^-$), necrotic (AX$^+$/PI$^+$), and total dead cell (AX$^+$%) population when compared with those of the sham. In comparison, TLR3$^{-/-}$ septic mice had no significant increase in splenocyte cell death compared with sham mice (Fig. 5, G and H). Finally, the spleen tissues isolated from TLR3$^{-/-}$ mice had less cleaved caspase-3 compared with that of WT after subjected to CLP, whereas the thymus protein lysates showed a similar level as that of WT (Fig. 5I), further suggesting that TLR3 deficiency attenuates cell death in the spleen induced by sepsis, similar to what ex vivo and in vivo imaging had revealed.

DISCUSSION

In a mouse model of polymicrobial sepsis, we tested in vivo fluorescent imaging of cell death in the thymus, spleen, and liver using NIR fluorochrome-labeled annexin V (AV-750). We found that the in situ fluorescent intensity of the thoracic and abdominal regions was markedly increased and dependent of sepsis severity. The increased fluorescent signal appeared to be the results of AV-750 accumulation in the thymus, spleen, and liver, respectively, as demonstrated by the ex vivo imaging of the isolated organs. The quantitative flow cytometry analysis of thymocytes and splenocytes revealed a significant number of cell death following sepsis, which was highly correlated with the in vivo fluorescent intensity of the thoracic and abdominal regions and the ex vivo fluorescent intensity of the septic thymus and spleen, respectively. Finally, we identified that systemic TLR3 deficiency attenuated cell death in the spleen but not in the thymus, as demonstrated by in vivo AV-750 imaging, by flow cytometry, and by cas-pase-3 cleavage when compared with WT mice during sepsis.

In order to test the utility of fluorescent AV-750 imaging to detect sepsis-induced cell death in vivo, we employed the well-established CLP model of sepsis (20, 21, 25) and confirmed the marked levels of apoptotic cell death in three main parenchymal organs, namely the liver,

spleen, and thymus. We used three different but complementary assays to detect apoptosis in these organs, including caspase-3 cleavage, caspase-3 activation, and TUNEL staining. These tests clearly demonstrated the significant amount of apoptosis in the liver, spleen, and thymus following sepsis.

We then tested the in vivo AV-750 imaging of the cell death in two mouse models of sepsis with mild and severe severity as defined by the levels of systemic cytokines, the levels of acute kidney injury biomarkers, and the overall mortality within 7 days. We found that the AV-750 fluorescent intensity in both thoracic and abdominal regions was markedly increased when compared with that of the sham animals and that the increase in the intensity was very much dependent of the sepsis severity. In the thoracic region, both mild and severe sepsis induced a significant increase in the annexin V fluorescence. The increased fluorescent signal was largely attributed to the septic thymus as demonstrated by the ex vivo imaging of the isolated thymus, where there was marked accumulation of annexin V compared with that of sham animals. The heart, the lung, and blood exhibited no significant fluorescent signal (Supplemental Fig. 1, Supplemental Digital Content 1, http://links.lww.com/CCM/B394), suggesting their minimal contribution to the thoracic fluorescent signal. Consistent with these imaging data, the flow cytometry analysis of the thymocytes isolated from these same animals revealed that there was a significant increase in the numbers of dying cells, both apoptotic (AX^+/PI^-) and necrotic (AX^+/PI^+) cells, in the thymus. Importantly, the intensity of both thoracic and thymus AV-750 imaging was highly correlated with the total number of thymocyte cell death as detected by flow cytometry. These data strongly suggest that sepsis, even in its mild form, induces a significant amount of cell death in the thymus and that the in vivo annexin V imaging is highly sensitive in detecting the dying thymocytes during sepsis.

In the abdominal region, we found that mice with severe sepsis exhibited a significant increase in the AV-750 fluorescent signal. Consistently, ex vivo imaging confirmed the enhanced AV-750 fluorescent signal in the liver and spleen of severe but not mild septic mice. Flow cytometry analysis of splenocytes demonstrated significant cell death in severe septic mice, which was well correlated with both abdominal and spleen fluorescent imaging strengths. Taken together, these data suggest that during severe sepsis, the abdominal imaging of AV-750 specifically detects the splenocyte cell death in vivo. Of importance, we noticed reduced bladder AV-750 signal in septic mice when compared with that of sham mice. This was most likely due to reduced urinary production caused by kidney hypoperfusion and acute kidney injury (25), consistent with the up-regulation of NGAL and KIM-1 (Fig. 2B). We further demonstrated the lack of AV-750 retention in the circulating blood 4 hours after IV injection in both sham and septic animals (Supplemental Fig. 1, A and C, Supplemental Digital Content 1, http://links.lww.com/CCM/B394), confirming that the enhanced AV-750 accumulation in the septic organs reflects increased lymphoid cell death, rather than increased retention of circulating AV-750 in the septic mice.

Lymphoid cell death occurs in the severe sepsis model. However, we found that lymphoid cell death also occurred in mild sepsis at 24 hours, suggesting significant lymphoid cell death during the onset of polymicrobial sepsis. Consistent with this is the significant lymphocytopenia in both mild and severe sepsis models. Drewry et al (13) reported a similar finding in patients whose absolute lymphocyte counts decrease to the similar levels in

survivors and nonsurvivors at the onset of sepsis and that nonsurvivors' absolute lymphocyte counts remain persistently low, whereas survivors experience lymphocyte recovery. Persistent lymphocytopenia on the fourth day of sepsis predicts early and late mortality (13). In our study, we were able to discriminate the mild and severe lymphoid cell death at 24 hours after CLP surgery by in vivo AV-750 imaging that was validated by ex vivo imaging, although both septic groups had similar levels of lymphocyte counts in their peripheral blood. These data suggest that the in vivo AV-750 imaging of lymphoid cell death provided additive and vital prognostic information.

TLR3 has been reported to play an important role in sepsis and serves as a sensor of tissue necrosis (33, 34). Here, we found that TLR3$^{-/-}$ septic mice had a significant lower AV-750 signal in the abdominal regions and in the spleen compared with WT septic mice, whereas similar AV-750 signal was present in the thymus of both TLR3$^{-/-}$ and WT septic mice. Once again, the in vivo and ex vivo AV-750 fluorescence data highly correlate with the data from flow cytometry and Western blot showing that TLR3$^{-/-}$ mice had significantly lower level of splenocyte cell death and less caspase cleavage, respectively, compared with WT mice. The finding that the lower level of cell death in TLR3$^{-/-}$ mice subjected to sepsis is consistent with a previous report by Cavassani et al (33) that shows that TLR3$^{-/-}$ septic mice have a marked reduction in necrotic peritoneal cells and a slight reduction in apoptotic peritoneal cells. The in vivo AV-750 fluorescent imaging in this study provides further information of lymphoid cell death in the deep organs and demonstrates further that TLR3 is involved in the cell death induced by polymicrobial sepsis.

The application of annexin V as a tool to detect cell death in vivo had been reported previously in cardiology (35–38) and oncology (39–41). NIR imaging is well suited to small animals but cannot be applied in humans due to limited penetration. With the development of radiolabeled derivatives of annexin V, in vivo imaging has been performed in patients and plays a significant role in evaluation of cell death and potential guidance of treatment (16, 37, 42). Radiolabeled versions of annexin, however, have been described and are under ongoing development. Initial versions of radiolabeled annexin were not site-modified, thus reducing annexin activity. This has now been overcome with several approaches (43, 44). Radiolabeled annexins have also been characterized by high background uptake in the abdomen, and new constructs with improved pharmacokinetics will need to be developed. Another limitation of the AV-750 imaging is from the metabolite of annexin V, which is cleared via the kidney and the liver. In this study, fluorescence-labeled annexin V shows low fluorescent signal in the abdominal area, which offers better target-to-background ratios and makes in vivo cell death imaging possible in the liver and spleen regions. Nevertheless, clinical translation of the approach described here is feasible and of significant potential.

Some limitations of this study should be noted. First, the study was conducted in mice. Although a strong annexin V signal in the thymus and significant thymocyte death are observed in septic mice, it is an unlikely case in humans because of marked thymus atrophy in human adults. Second, similar to other diseases, the mouse models may only provide partial information on human inflammation. There is an ongoing debate on the correlation of mouse models with human acute inflammatory conditions in the genomic responses (45–49). The study by Seok et al (45, 46) questions the utility of mouse models in predicting

specific genes/pathways in the human inflammatory diseases, such as sepsis, burn, and trauma. However, others raise the concerns about the methodology in the study and draw different and even opposite conclusions from the same genomic dataset (47, 49). Furthermore, it is worth noting that lymphatic cell death in sepsis has been well documented in both mouse models of sepsis and ICU patients with severe sepsis (8, 11). Therefore, it seems safe to state that the phenotype of lymphoid cell death observed in septic mice is shared by humans with severe sepsis.

In summary, we report here that in vivo AV-750 fluorescent imaging is feasible and exhibits good sensitivity in detecting cell death in the thymus, liver, and spleen during sepsis. We demonstrate that the AV-750 fluorescent intensity in the thoracic and upper abdominal fields is associated with sepsis severity and highly correlated with sepsis-induced cell death in the thymus and spleen, respectively. Thus, in vivo AV-750 imaging may represent a novel strategy to noninvasively detect sepsis-induced cell death in the lymphatic organs, monitor sepsis pathogenesis, and prognosis and facilitate an appropriate treatment.

Supplementary Material

Refer to Web version on PubMed Central for supplementary material.

ACKNOWLEDGMENT

REFERENCES

1. Minino AM, Heron MP, Murphy SL, et al.: Deaths: Final data for 2004. Natl Vital Stat Rep 2007; 55:1–119

2. Angus DC, Linde-Zwirble WT, Lidicker J, et al.: Epidemiology of severe sepsis in the United States: Analysis of incidence, outcome, and associated costs of care. Crit Care Med 2001; 29:1303–1310 [PubMed: 11445675]

3. Abraham E, Anzueto A, Gutierrez G, et al.: Double-blind randomised controlled trial of monoclonal antibody to human tumour necrosis factor in treatment of septic shock. NORASEPT II Study Group. Lancet 1998; 351:929–933 [PubMed: 9734938]

4. Angus DC, Crowther MA: Unraveling severe sepsis: Why did OPTIMIST fail and what's next? JAMA 2003; 290:256–258 [PubMed: 12851282]

5. Opal SM, Laterre PF, Francois B, et al.; ACCESS Study Group: Effect of eritoran, an antagonist of MD2-TLR4, on mortality in patients with severe sepsis: The ACCESS randomized trial. JAMA 2013; 309:1154–1162 [PubMed: 23512062]

6. Chung CS, Song GY, Lomas J, et al.: Inhibition of Fas/Fas ligand signaling improves septic survival: Differential effects on macrophage apoptotic and functional capacity. J Leukoc Biol 2003; 74:344–351 [PubMed: 12949237]

7. Hotchkiss RS, Swanson PE, Freeman BD, et al.: Apoptotic cell death in patients with sepsis, shock, and multiple organ dysfunction. Crit Care Med 1999; 27:1230–1251 [PubMed: 10446814]

8. Hotchkiss RS, Tinsley KW, Swanson PE, et al.: Sepsis-induced apoptosis causes progressive profound depletion of B and CD4+ T lymphocytes in humans. J Immunol 2001; 166:6952–6963 [PubMed: 11359857]

9. Hotchkiss RS, Karl IE: The pathophysiology and treatment of sepsis. N Engl J Med 2003; 348:138–150 [PubMed: 12519925]

10. Wesche-Soldato DE, Swan RZ, Chung CS, et al.: The apoptotic pathway as a therapeutic target in sepsis. Curr Drug Targets 2007; 8:493–500 [PubMed: 17430119]

11. Wesche-Soldato DE, Chung CS, Lomas-Neira J, et al.: In vivo delivery of caspase-8 or Fas siRNA improves the survival of septic mice. Blood 2005; 106:2295–2301 [PubMed: 15941915]

12. Hotchkiss RS, Coopersmith CM, McDunn JE, et al.: The sepsis seesaw: Tilting toward immunosuppression. Nat Med 2009; 15:496–497 [PubMed: 19424209]

13. Drewry AM, Samra N, Skrupky LP, et al.: Persistent lymphopenia after diagnosis of sepsis predicts mortality. Shock 2014; 42:383–391 [PubMed: 25051284]

14. Hotchkiss RS, Tinsley KW, Swanson PE, et al.: Prevention of lymphocyte cell death in sepsis improves survival in mice. Proc Natl Acad Sci U S A 1999; 96:14541–14546

15. Hotchkiss RS, Chang KC, Swanson PE, et al.: Caspase inhibitors improve survival in sepsis: A critical role of the lymphocyte. Nat Immunol 2000; 1:496–501 [PubMed: 11101871]

16. Boersma HH, Kietselaer BL, Stolk LM, et al.: Past, present, and future of annexin A5: From protein discovery to clinical applications. J Nucl Med 2005; 46:2035–2050 [PubMed: 16330568]

17. Balasubramanian K, Schroit AJ: Aminophospholipid asymmetry: A matter of life and death. Annu Rev Physiol 2003; 65:701–734 [PubMed: 12471163]

18. Martin SJ, Reutelingsperger CP, McGahon AJ, et al.: Early redistribution of plasma membrane phosphatidylserine is a general feature of apoptosis regardless of the initiating stimulus: Inhibition by overexpression of Bcl-2 and Abl. J Exp Med 1995; 182:1545–1556 [PubMed: 7595224]

19. Koopman G, Reutelingsperger CP, Kuijten GA, et al.: Annexin V for flow cytometric detection of phosphatidylserine expression on B cells undergoing apoptosis. Blood 1994; 84:1415–1420 [PubMed: 8068938]

20. Zou L, Feng Y, Chen YJ, et al.: Toll-like receptor 2 plays a critical role in cardiac dysfunction during polymicrobial sepsis. Crit Care Med 2010; 38:1335–1342 [PubMed: 20228680]

21. Zou L, Feng Y, Zhang M, et al.: Nonhematopoietic toll-like receptor 2 contributes to neutrophil and cardiac function impairment during polymicrobial sepsis. Shock 2011; 36:370–380 [PubMed: 21701420]

22. Rittirsch D, Huber-Lang MS, Flierl MA, et al.: Immunodesign of experimental sepsis by cecal ligation and puncture. Nat Protoc 2009; 4:31–36 [PubMed: 19131954]

23. Li Y, Si R, Feng Y, et al.: Myocardial ischemia activates an injurious innate immune signaling via cardiac heat shock protein 60 and toll-like receptor 4. J Biol Chem 2011; 286:31308–31319

24. Paragas N, Qiu A, Zhang Q, et al.: The Ngal reporter mouse detects the response of the kidney to injury in real time. Nat Med 2011; 17:216–222 [PubMed: 21240264]

25. Zou L, Feng Y, Li Y, et al.: Complement factor B is the downstream effector of TLRs and plays an important role in a mouse model of severe sepsis. J Immunol 2013; 191:5625–5635 [PubMed: 24154627]

26. Xiao H, Siddiqui J, Remick DG: Mechanisms of mortality in early and late sepsis. Infect Immun 2006; 74:5227–5235 [PubMed: 16926416]

27. Singleton KD, Wischmeyer PE: Distance of cecum ligated influences mortality, tumor necrosis factor-alpha and interleukin-6 expression following cecal ligation and puncture in the rat. Eur Surg Res 2003; 35:486–491 [PubMed: 14593232]

28. Doi K, Leelahavanichkul A, Yuen PS, et al.: Animal models of sepsis and sepsis-induced kidney injury. J Clin Invest 2009; 119:2868–2878 [PubMed: 19805915]

29. Zarjou A, Agarwal A: Sepsis and acute kidney injury. J Am Soc Nephrol 2011; 22:999–1006 [PubMed: 21566052]

30. Devarajan P: Review: Neutrophil gelatinase-associated lipocalin: A troponin-like biomarker for human acute kidney injury. Nephrology 2010; 15:419–428 [PubMed: 20609093]

31. Hardarson HS, Baker JS, Yang Z, et al.: Toll-like receptor 3 is an essential component of the innate stress response in virus-induced cardiac injury. Am J Physiol Heart Circ Physiol 2007; 292:H251–H258 [PubMed: 16936008]

32. Negishi H, Osawa T, Ogami K, et al.: A critical link between toll-like receptor 3 and type II interferon signaling pathways in antiviral innate immunity. Proc Natl Acad Sci U S A 2008; 105:20446–20451

33. Cavassani KA, Ishii M, Wen H, et al.: TLR3 is an endogenous sensor of tissue necrosis during acute inflammatory events. J Exp Med 2008; 205:2609–2621 [PubMed: 18838547]

34. Kaiser WJ, Sridharan H, Huang C, et al.: Toll-like receptor 3-mediated necrosis via TRIF, RIP3, and MLKL. J Biol Chem 2013; 288:31268–31279

35. Sosnovik DE, Schellenberger EA, Nahrendorf M, et al.: Magnetic resonance imaging of cardiomyocyte apoptosis with a novel magnetooptical nanoparticle. Magn Reson Med 2005; 54:718–724 [PubMed: 16086367]

36. Sosnovik DE, Nahrendorf M, Panizzi P, et al.: Molecular MRI detects low levels of cardiomyocyte apoptosis in a transgenic model of chronic heart failure. Circ Cardiovasc Imaging 2009; 2:468–475 [PubMed: 19920045]

37. Hofstra L, Liem IH, Dumont EA, et al.: Visualisation of cell death in vivo in patients with acute myocardial infarction. Lancet 2000; 356:209–212 [PubMed: 10963199]

38. Thimister PW, Hofstra L, Liem IH, et al.: In vivo detection of cell death in the area at risk in acute myocardial infarction. J Nucl Med 2003; 44:391–396 [PubMed: 12621005]

39. Belhocine T, Steinmetz N, Hustinx R, et al.: Increased uptake of the apoptosis-imaging agent (99m)Tc recombinant human Annexin V in human tumors after one course of chemotherapy as a predictor of tumor response and patient prognosis. Clin Cancer Res 2002; 8:2766–2774 [PubMed: 12231515]

40. Kartachova M, Haas RL, Olmos RA, et al.: In vivo imaging of apoptosis by 99mTc-Annexin V scintigraphy: Visual analysis in relation to treatment response. Radiother Oncol 2004; 72:333–339 [PubMed: 15450733]

41. Haas RL, de Jong D, Valdés Olmos RA, et al.: In vivo imaging of radiation-induced apoptosis in follicular lymphoma patients. Int J Radiat Oncol Biol Phys 2004; 59:782–787 [PubMed: 15183481]

42. Reutelingsperger C, Hofstra L: Visualisation of cell death. Lancet 2000; 356:2014

43. Fonge H, de Saint Hubert M, Vunckx K, et al.: Preliminary in vivo evaluation of a novel 99mTc-labeled HYNIC-cys-annexin A5 as an apoptosis imaging agent. Bioorg Med Chem Lett 2008; 18:3794–3798 [PubMed: 18524580]

44. Chen HH, Yuan H, Cho H, et al.: Cytoprotective nanoparticles by conjugation of a polyhis tagged annexin V to a nanoparticle drug. Nanoscale 2015; 7:2255–2259 [PubMed: 25572921]

45. Seok J, Warren HS, Cuenca AG, et al.; Inflammation and Host Response to Injury, Large Scale Collaborative Research Program: Genomic responses in mouse models poorly mimic human inflammatory diseases. Proc Natl Acad Sci U S A 2013; 110:3507–3512 [PubMed: 23401516]

46. Warren HS, Tompkins RG, Moldawer LL, et al.: Mice are not men. Proc Natl Acad Sci U S A 2015; 112:E345 [PubMed: 25540422]

47. Takao K, Miyakawa T: Genomic responses in mouse models greatly mimic human inflammatory diseases. Proc Natl Acad Sci U S A 2015; 112:1167–1172 [PubMed: 25092317]

48. Takao K, Hagihara H, Miyakawa T: Reply to Warren et al. and Shay et al.: Commonalities across species do exist and are potentially important. Proc Natl Acad Sci U S A 2015; 112:E347–E348 [PubMed: 25540421]

49. Shay T, Lederer JA, Benoist C: Genomic responses to inflammation in mouse models mimic humans: We concur, apples to oranges comparisons won't do. Proc Natl Acad Sci U S A 2015; 112:E346 [PubMed: 25540423]
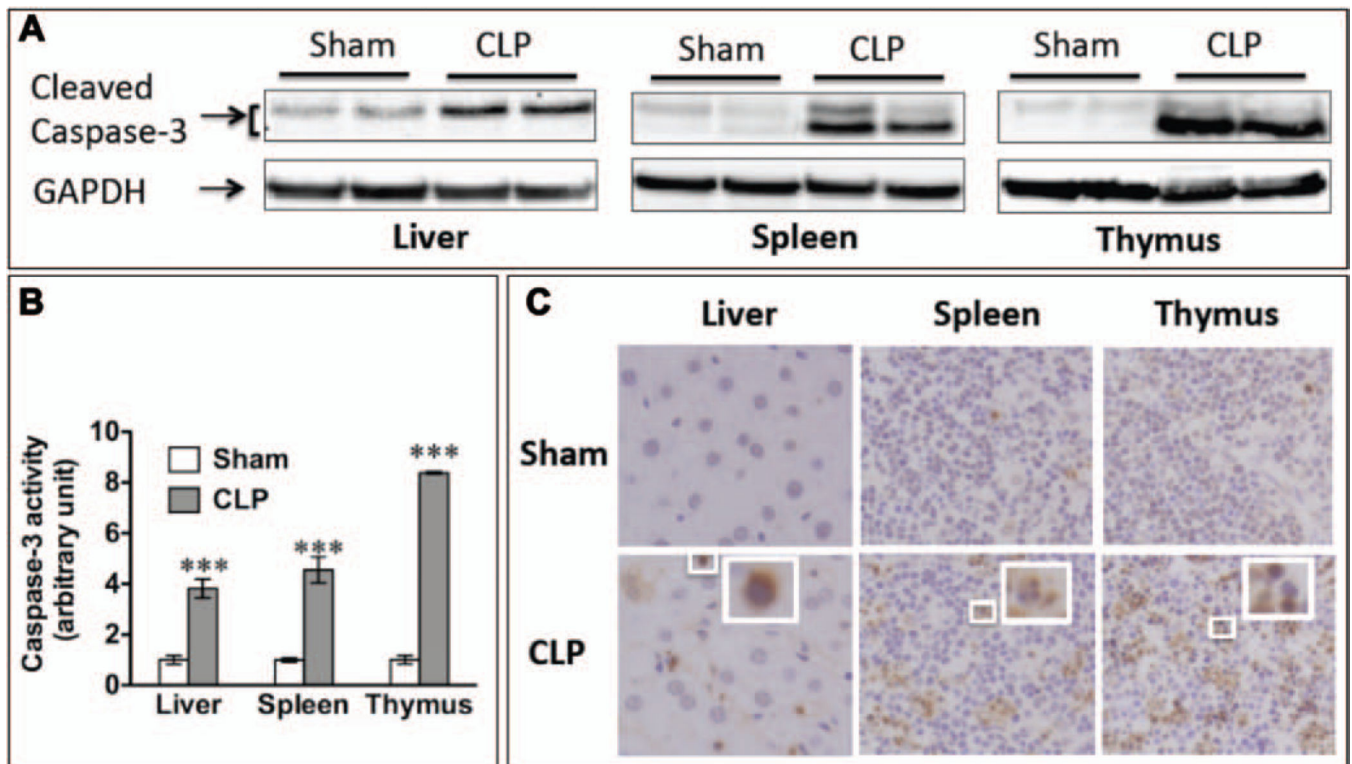
Figure 1.
Sepsis led to apoptosis in the liver, spleen, and thymus. Twenty-four hours after sham or cecum ligation and puncture (CLP) surgery (18-gauge needle), liver, spleen, and thymus were harvested and tested for apoptosis. **A**, CLP led to increased caspase-3 cleavage detected by Western blot. Glyceraldehyde 3-phosphate dehydrogenase (GAPDH) was employed as the internal control for equal protein loading. **B**, Caspase-3 activity was increased in septic organs. Fold change over the sham group was expressed. $n = 3$ in each group. ***$p < 0.001$ versus sham. **C**, Apoptosis occurred in the liver, spleen, and thymus as detected by terminal deoxynucleotidyl transferase dUTP nick-end labeling.
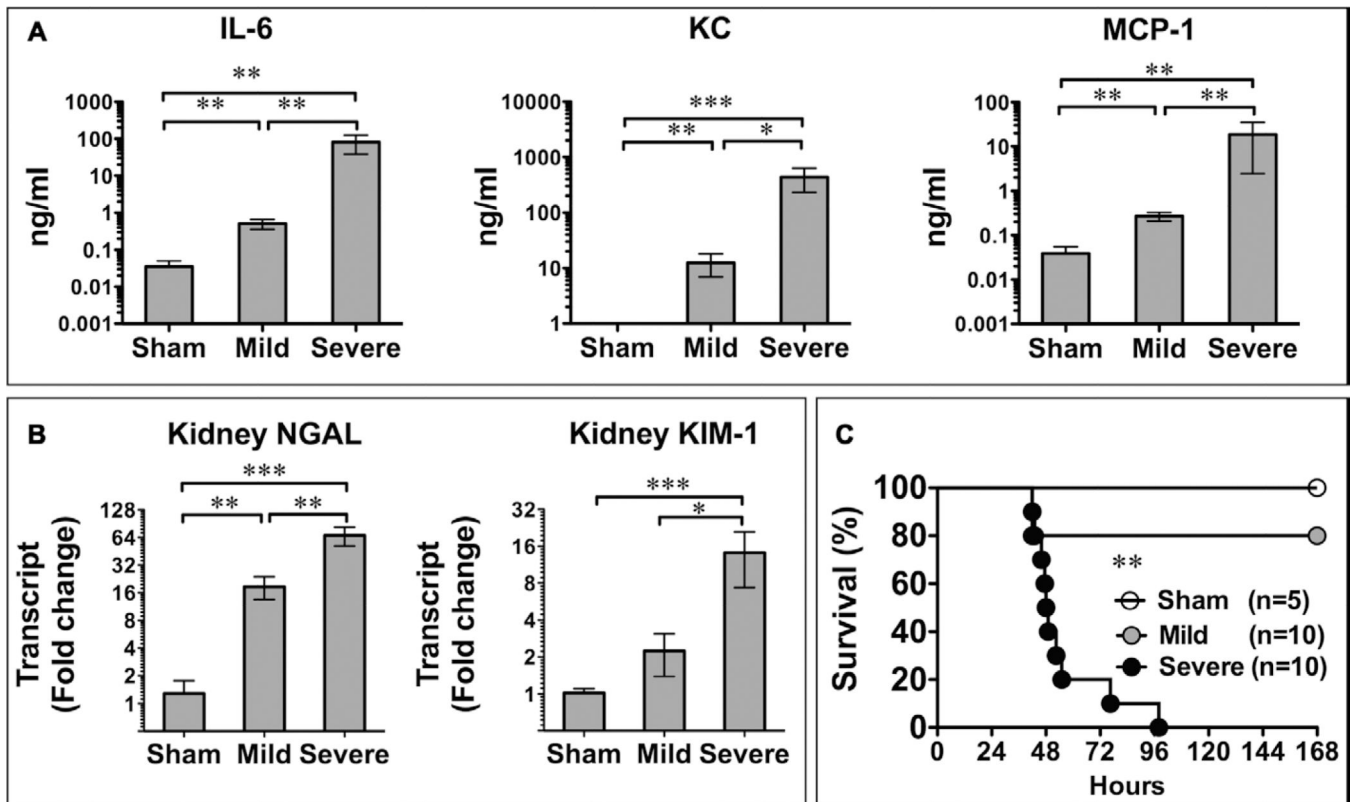
Figure 2.
Models of mild and severe sepsis. **A**, Serum cytokine 24 hr after surgery. Significant increases in interleukin (IL)-6, keratinocyte chemoattractant (KC), and monocyte chemoattractant protein (MCP)-1 were seen in a sepsis severity-dependent manner. *$p <$ 0.05, **$p < 0.01$, and ***$p < 0.001$. $n = 7$ in the sham group and $n = 6$ in mild and severe septic groups. **B**, Acute kidney injury developed in a severity-dependent manner. Neutrophil gelatinase–associated lipocalin (NGAL) and kidney injury molecule (KIM)-1 messenger RNA levels in the kidney were tested with quantitative reverse transcription-polymerase chain reaction 24 hr after surgery. *$p < 0.05$, **$p < 0.01$, and ***$p < 0.001$. $n = 7$ in each group. **C**, Survival rate of sham and septic mice. **$p < 0.01$ severe versus mild sepsis.
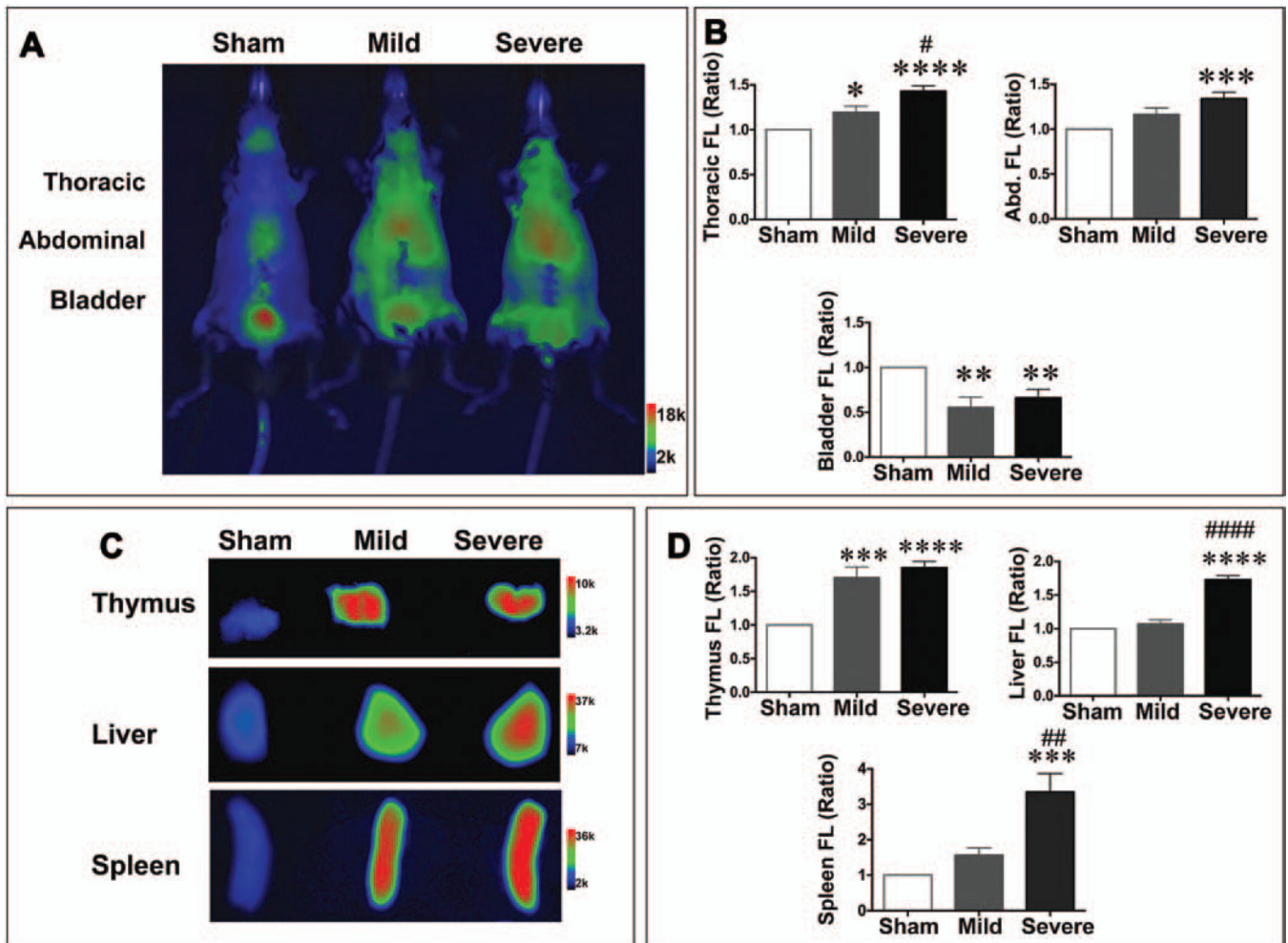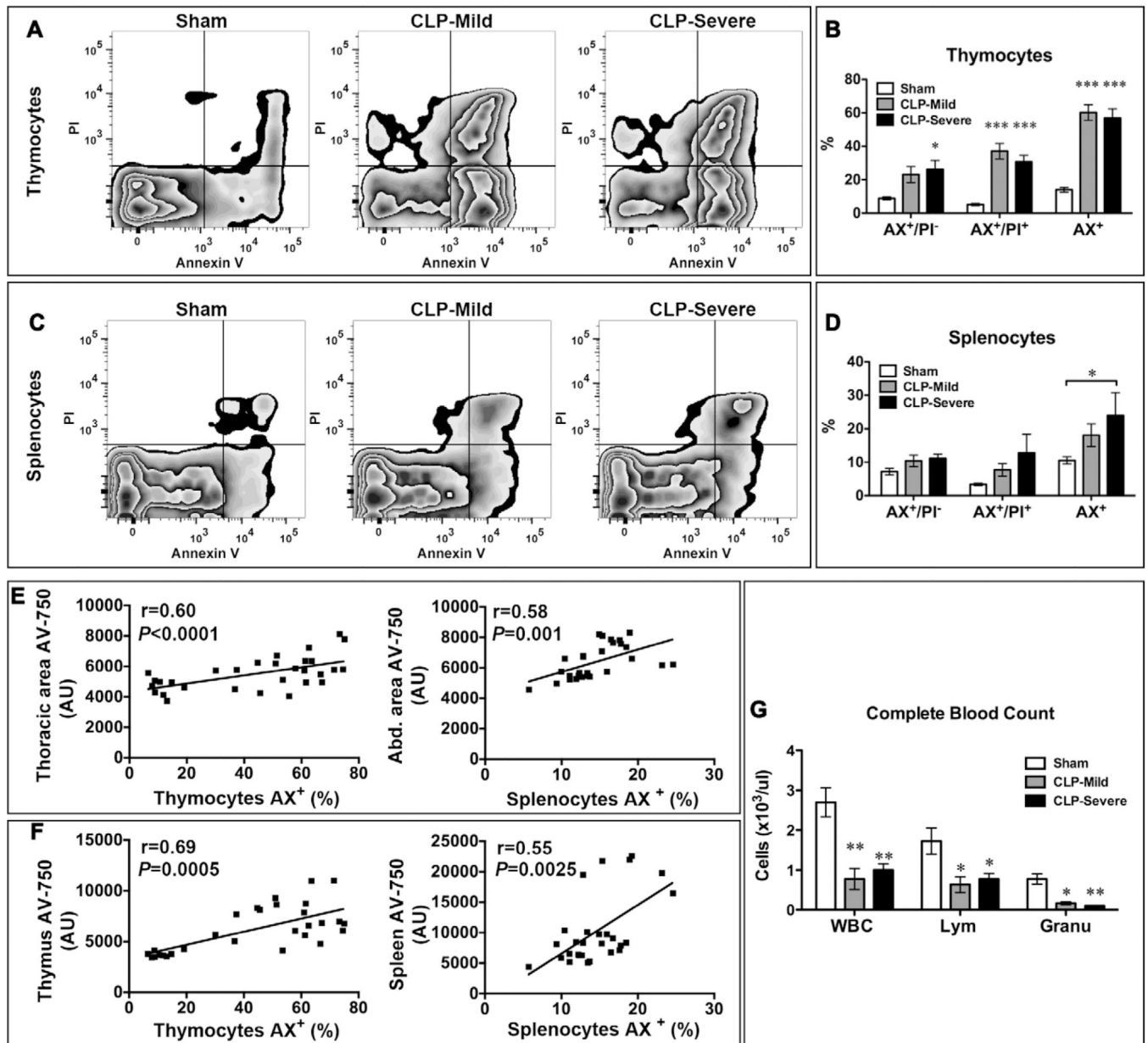
Figure 3.
Lymphoid cell death was detected in vivo and ex vivo with AV-750 imaging. Twenty hours after surgery, AV-750 dye was injected IV. Four hours later, mice were anesthetized and imaged in an IVIS imaging spectrum system. **A**, Representative AV-750 imaging in vivo in sham, mild, and severe groups. **B**, AV-750 fluorescence signal in vivo was quantified as ratio over sham. Probe uptake was significantly increased in sepsis in both the thorax and the abdominal regions. $n = 8$ in the sham group, $n = 6$ in the mild group, and $n = 8$ in the severe group. $*p < 0.05$, $***p < 0.001$, and $****p < 0.0001$ versus sham; $\#p < 0.05$ versus mild cecum ligation and puncture (CLP) group. **C**, Representative AV-750 imaging of the isolated thymus, liver, and spleen. **D**, Ex vivo AV-750 fluorescence signal was quantified as the ratio over sham. $**p < 0.01$, $***p < 0.001$, and $****p < 0.0001$ versus sham group. $\#\#p < 0.01$ and $\#\#\#\#p < 0.001$ versus mild CLP group. $n = 8$ in the sham group, $n = 6$ in the mild group, and $n = 8$ in the severe group. Abd. = abdominal, FL = fluorescence.

Figure 4.

Sepsis-induced lymphoid cell death correlates with AV-750 imaging in vivo and ex vivo. Right after AV-750 imaging, the thymi or spleens were gently ground to dissociate the cells. Thymocytes and splenocytes were stained with fluorescein-labeled annexin V (AX) and propidium iodide (PI). Flow cytometry were used to define the percentage of apoptosis, necrosis, and total cell death population. **A**, Representative picture of thymocyte flow cytometry. **B**, Mild and severe sepsis led to increased apoptosis (AX^+/PI^-), necrosis (AX^+/PI^+), and total cell death (AX^+) in thymocytes. $n = 5$ in the sham group and $n = 6$ in the CLP group. $*p < 0.05$ and $***p < 0.001$ versus sham. **C**, Representative picture of flow cytometry in splenocytes. **D**, Mild and severe sepsis increased splenocyte cell death. $n = 6$ in each group. $*p < 0.05$ versus sham. **E**, In vivo thoracic AV-750 signal correlates with thymocyte

cell death. In vivo abdominal AV-750 signal correlates with splenocyte cell death (AX^+, total cell death percentage; $n = 28$). **F**, Ex vivo imaging of AV-750 signal in the thymus and spleen correlates with thymocyte and splenocyte death, respectively (AX^+, total cell death percentage; $n = 28$). **G**, Complete blood count was tested 24 hr after surgery. $n = 4$ in each group. $*p < 0.05$ and $**p < 0.01$ versus sham. AU = arbitrary unit, CLP = cecum ligation and puncture, Granu = granulocyte, Lym = lymphocyte.
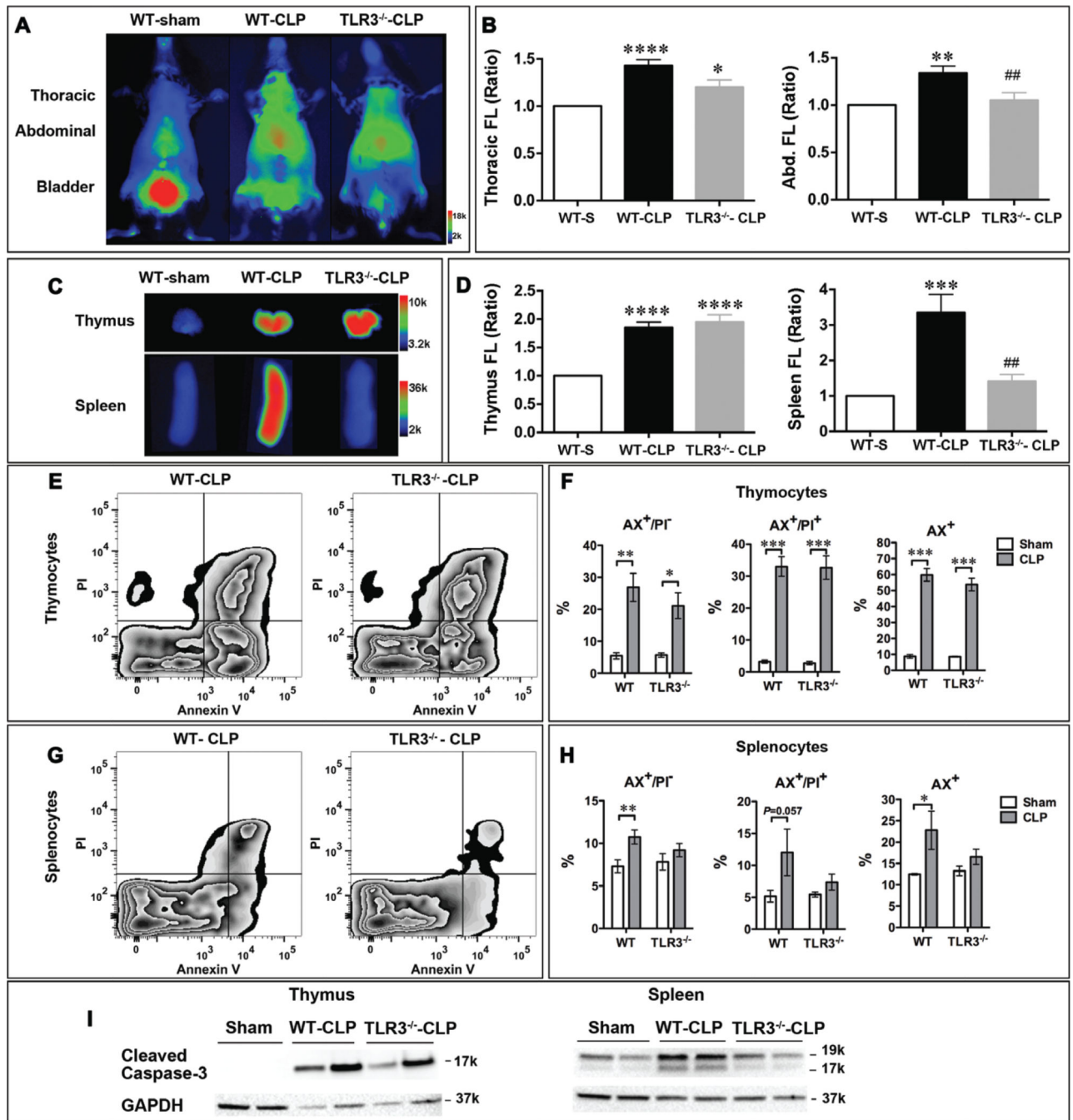
Figure 5.
Toll-like receptor 3 (TLR3) deficiency reduced cell death in the spleen. Wild-type (WT) and TLR3$^{-/-}$ mice were subjected to sham or cecum ligation and puncture (CLP) surgery (severe model). AV-750 imaging in vivo, organs ex vivo, and flow cytometry were applied to detect cell death at 24 hr. **A**, Representative pictures of in vivo AV-750 imaging. **B**, AV-750 fluorescence signal in vivo was quantified as ratio over sham. AV-750 uptake was significantly increased in sepsis in both the thorax and the abdominal regions. $*p < 0.05$, $**p < 0.01$, $***p < 0.001$, and $****p < 0.0001$ versus sham (WT-S). $\#\#p < 0.01$ versus WT-CLP.

$n = 3$ in the sham group, $n = 9$ in the WT-CLP group, and $n = 7$ in the TLR3$^{-/-}$-CLP group. **C**, Representative ex vivo AV-750 imaging. Right after in vivo imaging, thymus and spleen were harvested and exposed in an IVIS imaging system. **D**, Ex vivo AV-750 fluorescence signal is quantified as ratio over sham. ***$p < 0.001$ and ****$p < 0.0001$ versus sham (WT-S). $n = 3$ in the sham group, $n = 9$ in the WT-CLP group, and $n = 7$ in the TLR3$^{-/-}$-CLP group. ##$p < 0.01$ versus WT-CLP. **E**, Representative pictures of flow cytometry data in thymocytes. **F**, WT and TLR3$^{-/-}$ septic mice showed the same level of cell death in thymocytes. $n = 3$ in the sham group, $n = 9$ in the WT-CLP group, and $n = 7$ in the TLR3$^{-/-}$-CLP group group. *$p < 0.05$, **$p < 0.01$, and ***$p < 0.001$. **G**, Representative pictures of flow cytometry data in splenocytes. **H**, Sepsis led to cell death in WT splenocytes. *$p < 0.05$ and **$p < 0.01$. TLR3 deficiency prevented the development of splenocyte cell death induced by sepsis. $n = 3$ in the sham group, $n = 9$ in the WT-CLP group, and $n = 7$ in the TLR3$^{-/-}$-CLP group. **I**, Apoptosis was reduced in TLR3$^{-/-}$ septic spleen as evidenced by attenuated caspase-3 cleavage, but not in septic thymus. Glyceraldehyde-3-phosphate dehydrogenase (GAPDH) served as protein loading control. Abd. = abdominal, AX= fluorescein-labeled annexin V, FL = fluorescence, PI = propidium iodide.